Isotope effects in water as investigated by neutron diffraction and path integral molecular dynamics

Anita Zeidler[1], Philip S. Salmon[1], Henry E. Fischer[2], Jörg C. Neuefeind[3], J. Mike Simonson[4] and Thomas E. Markland[5]

[1] Department of Physics, University of Bath, Bath, BA2 7AY, UK
[2] Institut Laue-Langevin, 6 rue Jules Horowitz, BP 156, F-38042, Grenoble Cédex 9, France
[3] Spallation Neutron Source, Oak Ridge National Laboratory, Oak Ridge, Tennessee 37831, USA
[4] Center for Nanophase Materials Science, Oak Ridge National Laboratory, Oak Ridge, Tennessee 37831, USA
[5] Department of Chemistry, Stanford University, Stanford, California 94305, USA

Abstract. The structure of heavy and light water at 300 K was investigated by using a joint approach in which the method of neutron diffraction with oxygen isotope substitution was combined with path integral molecular dynamics simulations. The diffraction results, which give intra-molecular O-D and O-H bond distances of 0.985(5) and 0.990(5) Å, were found to be in best agreement with those obtained by using the flexible anharmonic TTM3-F water model. Both techniques show a difference of $\simeq$0.5% between the O-D and O-H intra-molecular bond lengths and the results support a competing quantum effects model for water in which its structural and dynamical properties are governed by an offset between intra-molecular and inter-molecular quantum contributions. Further consideration of the O-O correlations is needed in order to improve agreement with experiment.

PACS numbers: 61.05.fm, 61.20.Ja

1. Introduction

Liquid water is an essential substance having a plethora of important applications [1, 2]. There are, however, several elements of its structure and dynamics that remain hotly debated [2]. One aspect of the controversy is the role played by nuclear quantum effects, such as zero point energy and tunnelling, on water's hydrogen bonded network. This is manifested by differences between the structure and dynamics of heavy (D_2O) versus light (H_2O) water which lead to changes in properties such as their melting and boiling points, their temperature of maximum density, and their interaction with biological systems [2, 3, 4, 5, 6]. In addition, techniques such as two-dimensional infrared spectroscopy commonly require H to be partially substituted by D and hence it is important to understand the difference this engenders in the structure and dynamics of water [7, 8].

The method of neutron diffraction with H/D isotope substitution has provided important insight into the structure of water [9, 10, 11, 12]. Key to the application

of this technique is the assumption that there is a negligible difference between the structures of light and heavy water such that H and D are regarded as isomorphic. Differences between the structures of H_2O and D_2O have, however, been found from x-ray and gamma-ray diffraction experiments [3, 5, 13]. It is not, therefore, straight forward to gain additional information on the positions of hydrogen versus deuterium atoms by using neutron diffraction with H/D isotope substitution, although a scheme based on a linear combination of light and heavy water partial structure factors has been proposed [14]. Recently the bound coherent neutron scattering lengths of the oxygen isotopes have been re-measured by using the sensitive technique of neutron interferometry [15, 16, 17]. Importantly, a difference of 0.204(3) fm was observed between the scattering lengths of the isotope ^{18}O and oxygen of natural isotopic abundance $^{\rm nat}$O. This contrast, albeit small, is $\simeq$6 times greater than reported in standard tabulations of the neutron scattering lengths [18, 19, 20]. This suggests that it is possible to apply the method of neutron diffraction with oxygen isotope substitution to study the coordination environment of this element in disordered materials such as light and heavy water.

In the present paper we investigate the role of nuclear quantum effects on the structure of liquid water by using a joint approach in which the method of neutron diffraction with oxygen isotope substitution is combined with path integral molecular dynamics simulations. These simulations, in which a system of quantum mechanical particles is mapped onto a simulation of classical ring polymers, provide an exact treatment of nuclear quantum fluctuations in the structure of a given potential energy model for water [21]. In particular, we focus on the difference between the O-D and O-H intra-molecular bond distances in D_2O and H_2O and the implications this has for the proposal of "competing quantum effects" [4, 22], a notion that can be extended to other hydrogen bonded systems [23]. In view of the small size of the scattering length contrast between ^{18}O and $^{\rm nat}$O, a detailed account is given of the data acquisition and analysis procedures used for the neutron diffraction experiments. A brief account of the present work is reported elsewhere [16].

The manuscript is organized as follows. In section 2 we provide the essential theory needed to understand the neutron diffraction results. This is followed in section 3 by a description of the path integral molecular dynamics calculations. The experimental method is given in section 4 where particular attention is paid to the stability and reproducibility of the measured diffraction patterns. The experimental and path integral molecular dynamics results are presented in sections 5 and 6, respectively, and are discussed in section 7. Conclusions are drawn in section 8.

2. Neutron diffraction theory

In a reactor based neutron diffraction experiment on water, the incident wavelength λ is usually fixed and the diffracted intensity is measured as a function of the scattering angle 2θ [24]. The differential scattering cross section is related to the measured intensities by the expression (see e.g. [25])

$$\frac{{\rm d}\sigma}{{\rm d}\Omega} = \frac{1}{N_s A_{s,sc}(\theta)} \left\{ \left[\frac{I_{sc}(\theta)}{a(\theta)} - M_{sc}(\theta) \right] - \frac{A_{c,cs}(\theta)}{A_{c,c}(\theta)} \left[\frac{I_c(\theta)}{a(\theta)} - M_c(\theta) \right] \right\} \qquad (1)$$

where N_s represents the number of illuminated sample atoms and $a(\theta)$ is a normalization factor measured by reference to a vanadium standard [26]. $I_{sc}(\theta)$ and $I_c(\theta)$ are the intensities measured for the sample (s) in its container (c) and for the

empty container, respectively, which are corrected for background scattering at low 2θ values by reference to the intensity measured for a highly absorbing sample [27]. $A_{i,j}(\theta)$ denotes an attenuation factor which refers to neutrons that are scattered in medium i and attenuated, through absorption and scattering, in medium(s) j. $M_i(\theta)$ represents the cross section for multiple scattering in medium(s) i. For cylindrical samples, the $A_{i,j}(\theta)$ can be calculated by using the method of Paalman and Pings [28] and the $M_i(\theta)$ can be evaluated within the quasi-isotropic approximation by using the method of Soper and Egelstaff [29]. The procedure adopted in equation (1) ensures that the attenuation corrections are applied to once-scattered neutrons.

The differential scattering cross section given by equation (1) can also be written as

$$\mathrm{d}\sigma/\mathrm{d}\Omega = F(Q) + P(Q) \tag{2}$$

where the total structure factor, which contains information on the relative positions of pairs of distinct nuclei, is defined by

$$F(Q) = \sum_{\alpha=1}^{n}\sum_{\beta=1}^{n} c_\alpha c_\beta b_\alpha b_\beta \left[S_{\alpha\beta}(Q) - 1\right], \tag{3}$$

c_α and b_α are the atomic fraction and bound coherent neutron scattering length of chemical species α, $n = 2$ is the number of different chemical species, $S_{\alpha\beta}(Q)$ is a Faber-Ziman partial structure factor [30], and $Q = (4\pi/\lambda)\sin\theta$ is the magnitude of the scattering vector. The term $P(Q)$ contains a contribution from the self scattering from individual nuclei and a contribution from inelastic scattering, associated with both the self and distinct parts of $\mathrm{d}\sigma/\mathrm{d}\Omega$, for which there is no exact theory [24, 31, 32].

By making diffraction experiments on two samples of water that are identical in every respect, except that oxygen of natural isotopic abundance $^{\mathrm{nat}}$O is changed for the isotope ^{18}O, it is possible to simplify the complexity of correlations associated with $F(Q)$. For definiteness, let's consider two hydrogenated samples and let the same container in the same orientation be used to measure the scattered intensities which will be denoted by $I_{sc}(\theta)$ and $I'_{sc}(\theta)$. Since the samples differ only in the isotopic enrichment of the oxygen isotope, their scattering cross sections are very similar and their absorption cross sections are identical such that, on switching between them, there is very little change in either the magnitude or the 2θ dependence of $A_{s,sc}(\theta)$, $A_{c,cs}(\theta)$ or $M_{sc}(\theta)$. Specifically, the change on switching between $^{\mathrm{nat}}$O and ^{18}O enriched light water samples is $< 0.04\%$ for $A_{s,sc}(\theta)$, $< 0.025\%$ for $A_{c,cs}(\theta)$ and $\simeq 0.04\%$ for $M_{sc}(\theta)$. From equation (1) it follows that

$$\begin{aligned}\Delta F'_{\mathrm{H}}(Q) &\equiv \mathrm{d}\sigma/\mathrm{d}\Omega|^{18}_{\mathrm{H}} - \mathrm{d}\sigma/\mathrm{d}\Omega|^{\mathrm{nat}}_{\mathrm{H}} \\ &\cong \frac{1}{N_s A_{s,sc}(\theta)}\left[\frac{I'_{sc}(\theta) - I_{sc}(\theta)}{a(\theta)}\right]\end{aligned} \tag{4}$$

where superscripts denote the isotopic enrichment of oxygen and $A_{s,sc}(\theta)$ can be calculated for either one of the samples. Systematic errors arising from the container or multiple scattering (or background) corrections will, therefore, tend to cancel and the attenuation coefficient $A_{s,sc}(\theta)$ scales the difference $[I'_{sc}(\theta) - I_{sc}(\theta)]$ between the measured intensities. Thus, a strength of the difference function method is that it leads to a cancellation of many systematic errors, a fact that has been extensively exploited by Enderby, Neilson and co-workers in their pioneering work on aqueous ionic solutions [33, 34, 35]. We note that, while equation (4) demonstrates a key advantage of using

difference function methods, the full expressions for $\mathrm{d}\sigma/\mathrm{d}\Omega$ as given by equation (1) were used in our data analysis.

From equation (2) it follows that equation (4) can be re-written as

$$\Delta F'_{\mathrm{H}}(Q) = \Delta F_{\mathrm{H}}(Q) + \Delta P_{\mathrm{H}}(Q) \tag{5}$$

where the first difference function is given by

$$\begin{aligned}\Delta F_{\mathrm{H}}(Q) &= F_{\mathrm{H}}^{18}(Q) - F_{\mathrm{H}}^{\mathrm{nat}}(Q) \\ &= c_{\mathrm{O}}^2 \left(b_{^{18}\mathrm{O}}^2 - b_{^{\mathrm{nat}}\mathrm{O}}^2\right) \left[S_{\mathrm{OO}}(Q) - 1\right] + 2c_{\mathrm{O}}c_{\mathrm{H}}b_{\mathrm{H}} \left(b_{^{18}\mathrm{O}} - b_{^{\mathrm{nat}}\mathrm{O}}\right) \left[S_{\mathrm{OH}}(Q) - 1\right]\end{aligned} \tag{6}$$

while $b_{^{18}\mathrm{O}}$ and $b_{^{\mathrm{nat}}\mathrm{O}}$ are the neutron scattering lengths of ^{18}O and $^{\mathrm{nat}}$O, respectively. Thus the H-H correlations are eliminated on forming equation (5) and, since H nuclei are lighter than O nuclei and twice as numerous, the main contributions arising from inelastic scattering are also eliminated to leave a residual inelasticity correction $\Delta P_{\mathrm{H}}(Q)$. The corresponding real space information is obtained from the Fourier transform relation

$$\Delta G_{\mathrm{H}}(r) = \frac{1}{2\pi^2 \, n_0 \, r} \int_0^\infty \mathrm{d}Q \, Q \, \Delta F_{\mathrm{H}}(Q) \sin(Qr) \tag{7}$$

where n_0 is the atomic number density of the sample and r is a distance in real space. The expression for $\Delta G_{\mathrm{H}}(r)$ takes the same form as equation (6) but with the $S_{\alpha\beta}(Q)$ replaced by their corresponding partial pair distribution functions $g_{\alpha\beta}(r)$. The mean coordination number of atoms of type β, contained in a volume defined by two concentric spheres of radii r_i and r_j centred on an atom of type α, is given by

$$\bar{n}_{\alpha\beta} = 4\pi \, n_0 \, c_\beta \int_{r_i}^{r_j} \mathrm{d}r \, r^2 g_{\alpha\beta}(r). \tag{8}$$

For the case when both of the water samples are deuterated the relevant functions are denoted by

$$\Delta F'_{\mathrm{D}}(Q) = \Delta F_{\mathrm{D}}(Q) + \Delta P_{\mathrm{D}}(Q) \tag{9}$$

where the first difference function is given by

$$\begin{aligned}\Delta F_{\mathrm{D}}(Q) &= F_{\mathrm{D}}^{18}(Q) - F_{\mathrm{D}}^{\mathrm{nat}}(Q) \\ &= c_{\mathrm{O}}^2 \left(b_{^{18}\mathrm{O}}^2 - b_{^{\mathrm{nat}}\mathrm{O}}^2\right) \left[S_{\mathrm{OO}}(Q) - 1\right] + 2c_{\mathrm{O}}c_{\mathrm{D}}b_{\mathrm{D}} \left(b_{^{18}\mathrm{O}} - b_{^{\mathrm{nat}}\mathrm{O}}\right) \left[S_{\mathrm{OD}}(Q) - 1\right]\end{aligned} \tag{10}$$

and $\Delta P_{\mathrm{D}}(Q)$ is a residual inelasticity correction. $\Delta G_{\mathrm{D}}(r)$ takes the same form as equation (10) but with the $S_{\alpha\beta}(Q)$ replaced by their corresponding partial pair distribution functions $g_{\alpha\beta}(r)$.

It is also possible to simplify the complexity of correlations associated with a total structure factor by forming the second difference function

$$\Delta F_{\mathrm{OX}}(Q) = 1 + \frac{\Delta F'_{\mathrm{D}}(Q) - \Delta F'_{\mathrm{H}}(Q) - \Delta P_{\mathrm{OX}}(Q)}{2c_{\mathrm{O}}c_{\mathrm{H}} \left(b_{\mathrm{D}} - b_{\mathrm{H}}\right) \left(b_{^{18}\mathrm{O}} - b_{^{\mathrm{nat}}\mathrm{O}}\right)} \tag{11}$$

$$= 1 + \frac{\Delta F_{\mathrm{D}}(Q) - \Delta F_{\mathrm{H}}(Q)}{2c_{\mathrm{O}}c_{\mathrm{H}} \left(b_{\mathrm{D}} - b_{\mathrm{H}}\right) \left(b_{^{18}\mathrm{O}} - b_{^{\mathrm{nat}}\mathrm{O}}\right)} \tag{12}$$

where X represents a weighted average of H and D. $\Delta F_{\mathrm{OX}}(Q)$ corresponds to $S_{\mathrm{OD}}(Q)$ (or $S_{\mathrm{OH}}(Q)$) if the net quantum effects are sufficiently small that there is good cancellation of the $S_{\mathrm{OO}}(Q)$ functions for light and heavy water and $S_{\mathrm{OH}}(Q) \simeq S_{\mathrm{OD}}(Q)$. The residual inelasticity correction $\Delta P_{\mathrm{OX}}(Q) = \Delta P_{\mathrm{D}}(Q) - \Delta P_{\mathrm{H}}(Q)$ is particularly small because the inelasticity corrections on the first difference functions have the same sign and are comparable in magnitude (see section 5.1).

It is also instructive to form the weighted difference function

$$\Delta F_{\mathrm{OO}}(Q) = 1 + \frac{\Delta F'_{\mathrm{D}}(Q) - [b_{\mathrm{D}}\Delta F'_{\mathrm{H}}(Q)/b_{\mathrm{H}}] - \Delta P_{\mathrm{OO}}(Q)}{c_{\mathrm{O}}^2\,(1 - b_{\mathrm{D}}/b_{\mathrm{H}})\left(b_{^{\mathrm{is}}\mathrm{O}}^2 - b_{^{\mathrm{nat}}\mathrm{O}}^2\right)} \tag{13}$$

$$= 1 + \frac{\Delta F_{\mathrm{D}}(Q) - [b_{\mathrm{D}}\Delta F_{\mathrm{H}}(Q)/b_{\mathrm{H}}]}{c_{\mathrm{O}}^2\,(1 - b_{\mathrm{D}}/b_{\mathrm{H}})\left(b_{^{\mathrm{is}}\mathrm{O}}^2 - b_{^{\mathrm{nat}}\mathrm{O}}^2\right)} \tag{14}$$

which is equal to $S_{\mathrm{OO}}(Q)$ in the limit when D and H are sufficiently isomorphic that the structures of H_2O and D_2O are identical. The inelasticity correction is given by $\Delta P_{\mathrm{OO}}(Q) = \Delta P_{\mathrm{D}}(Q) - [b_{\mathrm{D}}\Delta P_{\mathrm{H}}(Q)/b_{\mathrm{H}}]$ and, since the ratio $b_{\mathrm{D}}/b_{\mathrm{H}} = -1.769(1)$ (see section 4) and the inelasticity corrections on the first difference functions have the same sign and are comparable in magnitude, the latter do not tend to cancel as in the case of $\Delta F_{\mathrm{OX}}(Q)$. It follows that $\Delta P_{\mathrm{OX}}(Q) \ll \Delta P_{\mathrm{H}}(Q) \sim \Delta P_{\mathrm{D}}(Q) \ll \Delta P_{\mathrm{OO}}(Q)$ such that, in practice, it is more difficult to accurately measure $\Delta F_{\mathrm{OO}}(Q)$.

The real space functions corresponding to $\Delta F_{\mathrm{OX}}(Q)$ and $\Delta F_{\mathrm{OO}}(Q)$ are denoted by $\Delta G_{\mathrm{OX}}(r)$ and $\Delta G_{\mathrm{OO}}(r)$. In the limit when quantum effects are negligible, the latter are equal to $g_{\mathrm{OH}}(r)$ (or $g_{\mathrm{OD}}(r)$) and $g_{\mathrm{OO}}(r)$, respectively.

3. Path integral molecular dynamics

The path integral molecular dynamics simulations [21] were performed for several common models of water, namely the rigid models TIP4P [36] and SPC/E [37], the flexible harmonic models SPC/F [38] and qSPC/Fw [39], and the flexible anharmonic models q-TIP4P/F [22] and TTM3-F [40]. Each simulation was made for a system of 1000 water molecules (3000 atoms) using 32 imaginary time replicas at a temperature of 300 K and for an atomic number density $n_0 = 0.100$ Å^{-3}. Periodic boundary conditions were applied using the minimum image convention. The equations of motion were integrated using a time step of 0.75 fs and the properties for light and heavy water were each obtained from simulations totalling 1.5 ns. The simulation temperature was controlled using the path integral Langevin equation approach [41] and the ring polymer contraction scheme [42] was used to accelerate convergence. The simulations gave results that were converged to graphical accuracy.

4. Experimental method

The neutron diffraction experiments were made using the instrument D4c [43, 44] at the Institut Laue-Langevin with an incident wavelength of $\simeq 0.5$ Å at a temperature $T = 300.6(5)$ K. The heavy water samples were $D_2{}^{\mathrm{nat}}O$ and $D_2{}^{18}O$ (1.82% ^{16}O, 0.50% ^{17}O and 97.68 % ^{18}O) supplied by Euriso-top with a D:H ratio of 0.9947: 0.0053. Several other $D_2{}^{\mathrm{nat}}O$ samples were run with different D:H ratios in the range 0.9988:0.0012–0.9921:0.0079 to investigate the effect of the deuteration level on the final results. The light water samples were $H_2{}^{\mathrm{nat}}O$ and $H_2{}^{18}O$ (Euriso-top, 1.4% ^{16}O, 0.5% ^{17}O and 98.1% ^{18}O). The reproducibility of the light water results was checked by making two independent experiments a year apart. The samples were handled in a dry (< 4 ppm water) argon filled glove box.

The same cylindrical thin walled (0.1 mm) vanadium container (internal radius 2.4 mm) was used to hold the samples for the diffraction experiments and, for a given experiment, it was always mounted in the same orientation. Diffraction patterns were taken for each sample in its container, the empty container, and a cylindrical

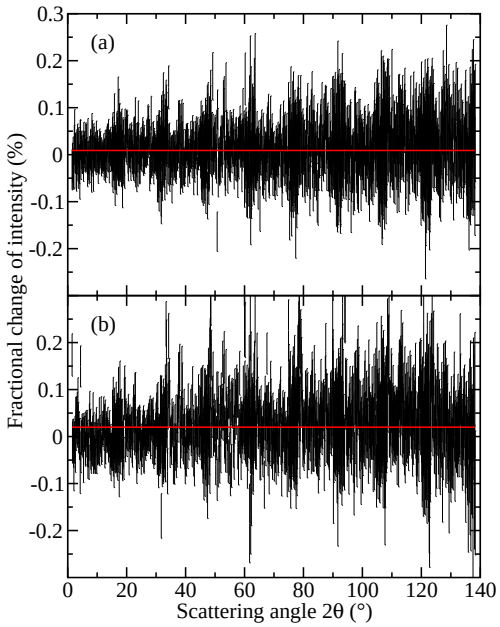

Figure 1. The stability and reproducibility of the diffraction patterns measured by using D4c [43, 44]. (a) The stability was assessed from the fractional change of intensity between the first and second halves of the data acquisition for the same mounting of a given sample. The data taken for a sample of $H_2{}^{18}O$ in its vanadium container are illustrated. The acquisition time for the first and second half intensities, $I_{sc,1}(\theta)$ and $I_{sc,2}(\theta)$, was ∼13.5 h each and the function $(I_{sc,2}(\theta) - I_{sc,1}(\theta))/(I_{sc,1}(\theta) + I_{sc,2}(\theta))$ is plotted as data points with vertical error bars. The fractional change of intensity shows no 2θ dependence within the statistical uncertainty and the fit to a constant level (horizontal solid light (red) curve) gives a value of 0.009(1)%. (b) The reproducibility was assessed from the fractional change of intensity between the diffraction patterns measured for two different mountings of a sample of $H_2{}^{nat}O$ in the same vanadium container. The acquisition times for the intensities $I'_{sc,1}(\theta)$ and $I'_{sc,2}(\theta)$ measured in the first and second mountings were ∼10 and ∼15.5 h, respectively, and the function $(I'_{sc,2}(\theta) - I'_{sc,1}(\theta))/(I'_{sc,1}(\theta) + I'_{sc,2}(\theta))$ is plotted as data points with vertical error bars. The fractional change of intensity shows no 2θ dependence within the statistical uncertainty and the fit to a constant level (horizontal solid light (red) curve) gives a value of 0.020(1)%. In (a) and (b) the data points show 8 bands of higher density error bars in 2θ which correspond to the overlap regions between the 9 D4c multi-detectors.

vanadium rod of diameter 6.37 mm for normalisation purposes. The intensity for a bar of neutron absorbing $^{10}B_4C$ of dimensions comparable to the sample was also measured to account for the effect of the sample's attenuation on the background signal at small scattering angles [27]. The stability and reproducibility of the diffraction patterns was assessed by using the procedure outlined in section 4.1 and the data sets were corrected by using the procedure described in section 2. The atomic number density $n_0 = 0.100$ Å^{-3}.

The neutron scattering lengths, taking into account the isotopic enrichment of

the isotopes, are $b_{^{18}\mathrm{O}} = 6.005(5)$ fm, $b_{^{\mathrm{nat}}\mathrm{O}} = 5.805(4)$ fm, $b_{\mathrm{D}} = 6.619(6)$ fm and $b_{\mathrm{H}} = -3.7409(11)$ fm. The weighting factors for the $[S_{\mathrm{OO}}(Q) - 1]$ term in equations (6) and (10) are therefore 0.00263(8) and 0.00262(8) barn, respectively, whereas the weighting factors for the $[S_{\mathrm{OH}}(Q) - 1]$ and $[S_{\mathrm{OD}}(Q) - 1]$ terms in these equations are $-0.0033(1)$ and 0.0059(2) barn, respectively. The O-H correlations receive a negative weighting factor on account of the negative value of b_{H}. The cross sections used for the attenuation and multiple scattering corrections were based on the measured values at an incident neutron wavelength of 0.5 Å and are 17.1(4) and 3.6(1) barn atom^{-1} for light and heavy water of natural isotopic abundance, respectively [45].

4.1. Stability and reproducibility of the measured diffraction patterns

Each complete diffraction pattern was built up from the intensities measured for different positions of the group of nine microstrip detectors on D4c [44]. The stability of the diffractometer was assessed by finding the fractional change of intensity between successive diffraction patterns measured for the same mounting of a sample in the instrument. For each sample, the fractional change of intensity showed no 2θ dependence within the statistical uncertainty so that the data could be fitted to a constant level (figure 1(a)). The mean fractional change of intensity for the various samples was found to be $\pm 0.0071(4)\%$ or $\pm 0.012(8)\%$, depending on whether or not the experimental uncertainties on the fitted levels were used to weight the measured data sets, respectively. The values are consistent with the quoted count rate stability for D4c of $\pm 0.01\%$ over three days [43, 44].

The reproducibility of the diffraction data was assessed by measuring the diffraction patterns for two different mountings of a sample of $\mathrm{H_2}^{\mathrm{nat}}\mathrm{O}$. After the first diffraction pattern was measured, the sample was dismounted and removed from its vanadium container which was subsequently used for other diffraction measurements. Two days later, the container was reloaded with sample, remounted and a second diffraction pattern was measured. The fractional change of intensity showed no 2θ dependence within the statistical uncertainty and the fit to a constant level gave a value of $0.020(1)\%$ (figure 1(b)).

5. Experimental results

5.1. First difference functions $\Delta F_{\mathrm{D}}(Q)$ and $\Delta F_{\mathrm{H}}(Q)$

The measured differential scattering cross sections, $\mathrm{d}\sigma/\mathrm{d}\Omega$, for the heavy and light water samples are shown in figure 2. There is a small but significant contrast between the measured data sets as shown by the the first difference functions $\Delta F'_{\mathrm{D}}(Q)$ and $\Delta F'_{\mathrm{H}}(Q)$ illustrated in figure 3. The slope on each of these first difference functions arises from residual inelasticity effects and is positive in accordance with the larger mass of $^{18}\mathrm{O}$ compared to $^{\mathrm{nat}}\mathrm{O}$.

The residual inelasticity corrections were obtained by using the expression $\Delta P(Q) = a + bQ^2 + cQ^4$ where, in practice, the coefficients a, b and c were obtained by fitting $Q\Delta P_{\mathrm{D}}(Q)$ to $Q\Delta F'_{\mathrm{D}}(Q)$ or by fitting $Q\Delta P_{\mathrm{H}}(Q)$ to $Q\Delta F'_{\mathrm{H}}(Q)$. In the absence of an exact theory for the inelasticity corrections for water [24, 31, 32], it is difficult to assess the accuracy of the approximation chosen for $\Delta P(Q)$ which is valid for nuclei that are heavy by comparison with the neutron [46]. However, the first difference functions eliminate the significant contribution arising from either the H-H or D-D

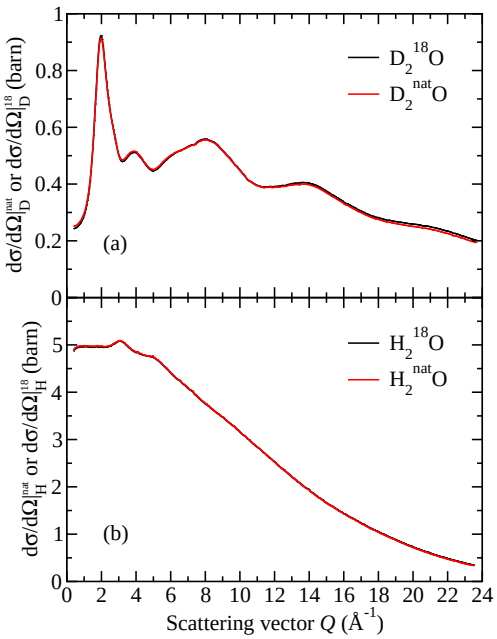

Figure 2. The differential scattering cross sections, $d\sigma/d\Omega$, as obtained from the diffraction patterns measured for samples of (a) $D_2{}^{nat}O$ and $D_2{}^{18}O$ or (b) $H_2{}^{nat}O$ and $H_2{}^{18}O$. The error bars are much smaller than the thickness of a line. The slope on each data set arises from inelasticity effects and is more pronounced the lighter the nuclei.

correlations and the remaining contributions involve oxygen nuclei that are relatively heavy. Also, it is anticipated that any remaining correction will be a small-amplitude gently-varying function of Q that will not materially affect e.g. the Q space oscillations giving rise to the intra-molecular O-D peak or O-H trough in real space. As shown below, this hypothesis was verified in the case of heavy water by varying the D:H ratio for the $D_2{}^{nat}O$ sample. The correction terms $\Delta P_D(Q)$ and $\Delta P_H(Q)$ are shown in figure 3 and the slope corrected first difference functions $\Delta F_D(Q)$ and $\Delta F_H(Q)$ are given in figures 4 and 5, respectively. It is worthwhile emphasizing that these functions were not obtained by using smoothed data sets i.e. the data analysis was made point by point. This statement can be verified by comparing the magnitude of the error bars with the distribution of data points. The measured functions show both internal and external consistency [47].

The real space functions $\Delta G_D(r)$ and $\Delta G_H(r)$ were obtained by spline fitting $\Delta F_D(Q)$ and $\Delta F_H(Q)$ and Fourier transforming, before and after the application of a Lorch [48, 49] modification function. The data obtained from the first procedure were joined smoothly to the data obtained from the second procedure at a point just beyond the first peak or trough in real space [16]. The resultant functions are shown in figure 6. The first peak in $\Delta G_D(r)$ at 0.985(5) Å and the first trough in $\Delta G_H(r)$ at 0.990(5) Å arise from intra-molecular O-D and O-H correlations and give coordination numbers of

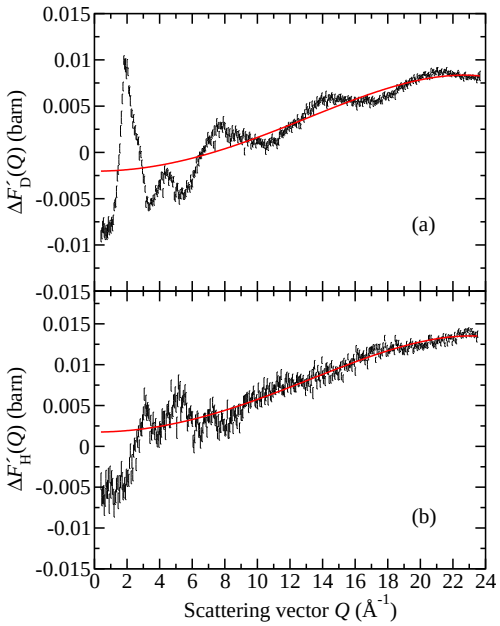

Figure 3. The first difference functions (a) $\Delta F'_{\rm D}(Q)$ and (b) $\Delta F'_{\rm H}(Q)$ before the application of a correction for residual inelasticity effects. The vertical bars give the statistical errors on the data points and the solid (red) curves give the fitted residual inelasticity corrections $\Delta P_{\rm D}(Q)$ and $\Delta P_{\rm H}(Q)$.

$\bar{n}_{\rm OD} = 1.9(1)$ and $\bar{n}_{\rm OH} = 2.0(2)$. The O-D distance compares with a value of 0.983(8) Å obtained by Powles [31] from a re-analysis of neutron diffraction data for liquid heavy water at 294 K. By comparison, in ice-Ih at 123 K a combination of crystallographic, nuclear magnetic resonance and spectroscopic results point to O-D and O-H distances of 0.983(5) and 0.987(5) Å, respectively, which are in agreement with the values we obtain for the liquid phase [50]. The O-D distance has also been estimated to be 0.985(7) Å from a pair distribution function analysis of neutron diffraction data for ice-Ih [51]. In the vapor phase of water in its ground vibrational state, an analysis of infra-red and microwave spectroscopy data give O-D and O-H distances of 0.9687 and 0.9724 Å, respectively [52]. The difference between the O-D and O-H bond lengths of $\simeq$0.5% that we observe for the liquid phase therefore compares to $\simeq$0.4% for both the ambient pressure crystalline and vapor phases of water. All of the latter are much smaller than the difference of $\sim$3% found in the most recent modelling of neutron and x-ray data for liquid water [54], a difference that is also much larger than found in any theoretical prediction (see section 7.1).

In the case of heavy water, the robustness of the results was assessed by measuring the diffraction patterns for $D_2{}^{18}O$ and for several $D_2{}^{\rm nat}O$ samples with different D:H ratios in the range from 0.9988:0.0012 to 0.9921:0.0079. The $\Delta F'_{\rm D}(Q)$ functions obtained from these data sets are shown in figure 7. The slope from the residual inelasticity correction, $\Delta P_{\rm D}(Q)$, is positive for most of the functions since ^{18}O has a larger mass compared to $^{\rm nat}$O. The slope is, however, negative in the case of

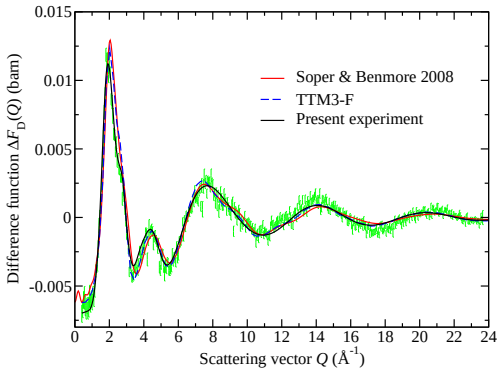

Figure 4. The first difference function $\Delta F_{\rm D}(Q)$ as obtained from the present experiment (points with vertical (green) error bars), from the EPSR model of Soper and Benmore [54] (solid light (red) curve), and from the path integral molecular dynamics simulation for the TTM3-F model (broken dark (blue) curve). The solid dark (black) curve gives the Fourier back transform of the $\Delta G_{\rm D}(r)$ function shown by the solid dark (black) curve in figure 6 where the unphysical oscillations at r values smaller than the distance of closest approach between the centres of two atoms are set to the calculated limit for $\Delta G_{\rm D}(r = 0)$.

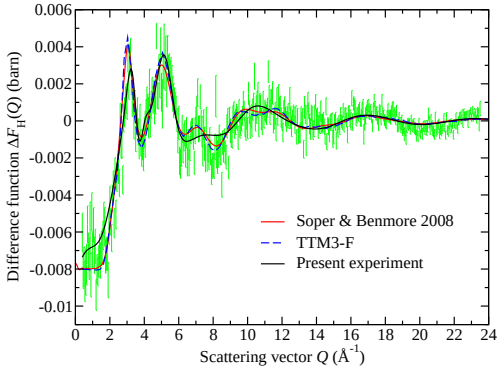

Figure 5. The first difference function $\Delta F_{\rm H}(Q)$ as obtained from the present experiment (points with vertical (green) error bars), from the EPSR model of Soper and Benmore [54] (solid light (red) curve), and from the path integral molecular dynamics simulation for the TTM3-F model (broken dark (blue) curve). The solid dark (black) curve gives the Fourier back transform of the $\Delta G_{\rm H}(r)$ function shown by the solid dark (black) curve in figure 6 where the unphysical oscillations at r values smaller than the distance of closest approach between the centres of two atoms are set to the calculated limit for $\Delta G_{\rm H}(r = 0)$.

the $\Delta F'_{\rm D}(Q)$ function formed by using the data measured for the $D_2{}^{\rm nat}O$ sample with 99.88% D since this has a relatively large imbalance with the light hydrogen content of the $D_2{}^{18}O$ sample. After the correction for $\Delta P_{\rm D}(Q)$ is made, several of the

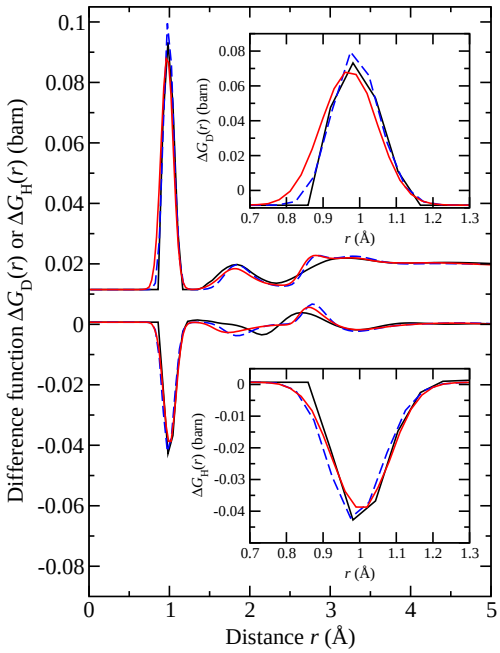

Figure 6. The first difference functions $\Delta G_{\rm D}(r)$ and $\Delta G_{\rm H}(r)$ for heavy and light water as obtained from the present experiment (solid dark (black) curves), from the EPSR models of Soper and Benmore [54] (solid light (red) curves), and from the path integral molecular dynamics simulations using the TTM3-F model (broken dark (blue) curves). The data sets for $\Delta G_{\rm D}(r)$ (top set of curves) have been shifted upward by 0.02 barn. The insets show in more detail the region of the first peak in $\Delta G_{\rm D}(r)$ or the first trough in $\Delta G_{\rm H}(r)$.

corresponding real space data sets $\Delta G_{\rm D}(r)$ are shown in figure 8. It is found that a 0.2% change in the D content alters $\Delta P_{\rm D}(Q)$ but does not have a material effect on the results for $\Delta F_{\rm D}(Q)$. In particular, the comparison made in figure 8 shows that all of the main features in $\Delta G_{\rm D}(r)$ are reproducible and the intra-molecular O-D peak has a position in the range 0.985±0.005 Å.

In the case of light water, the reproducibility of the results was assessed by making two independent diffraction experiments a year apart. The reciprocal space functions were found to be in agreement within the experimental error and the results showed that the first trough in real space, resulting from intra-molecular O-H correlations, is a robust feature with a position in the range 0.990±0.005 Å. The higher r features were, however, found to be more sensitive to the effects of noise in reciprocal space and, while these effects were reduced by combining the data sets to give the weighted average shown in figure 5, the higher r features in $\Delta G_{\rm H}(r)$ are not as reliable as the corresponding features in $\Delta G_{\rm D}(r)$.

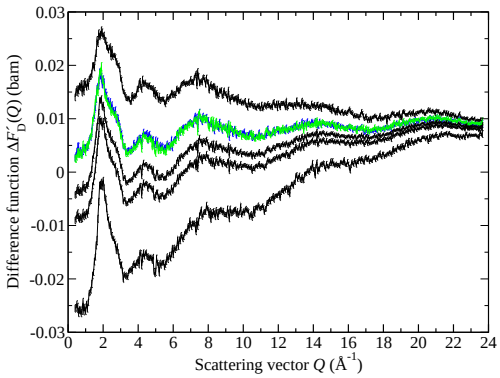

Figure 7. The first difference functions $\Delta F'_{\mathrm{D}}(Q)$ as obtained from the measured diffraction pattern for a sample of $D_2{}^{18}O$ with a D:H ratio of 0.9947:0.0053 and for several samples of $D_2{}^{\mathrm{nat}}O$ having different D:H ratios of (from top to bottom) 0.9988:0.0012, 0.9966:0.0034 (blue), 0.9964:0.0036 (green), 0.9954:0.0046, 0.9947:0.0053 and 0.9921:0.0079. The vertical bars give the statistical errors on the data points.

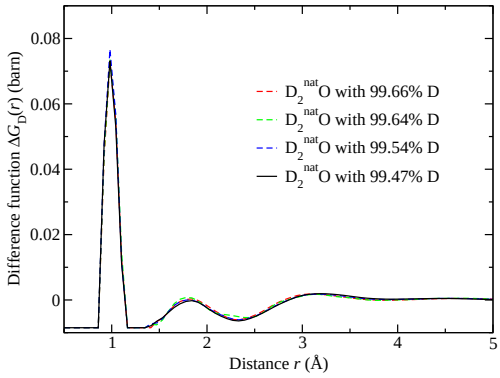

Figure 8. The first difference functions $\Delta G_{\mathrm{D}}(r)$ as obtained by Fourier transforming several of the slope corrected $\Delta F'_{\mathrm{D}}(Q)$ functions shown in figure 7 that were constructed by combining the measured diffraction pattern for $D_2{}^{18}O$ with the measured diffraction pattern for several samples of $D_2{}^{\mathrm{nat}}O$ having different D:H ratios. The different $\Delta P_{\mathrm{D}}(Q)$ corrections, arising from the different D:H ratios chosen for the $D_2{}^{\mathrm{nat}}O$ samples, have little effect on $\Delta G_{\mathrm{D}}(r)$ and the first peak, which is attributable to intra-molecular O-D correlations, has a position in the range 0.985±0.005 Å.

5.2. Second difference function $\Delta F_{\mathrm{OX}}(Q)$

The second difference function $\Delta F_{\mathrm{OX}}(Q)$ illustrated in figure 9 was constructed from the $\Delta F_{\mathrm{D}}(Q)$ and $\Delta F_{\mathrm{H}}(Q)$ functions shown in figures 4 and 5 by using equation (12).

It was checked that the same $\Delta F_{\rm OX}(Q)$ function was obtained, within the statistical errors, by fitting the difference $[\Delta F'_{\rm D}(Q) - \Delta F'_{\rm H}(Q)]$ to the expression $\Delta P_{\rm OX}(Q) = a + bQ^2 + cQ^4$ and by combining the results according to equation (11). The real space function $\Delta G_{\rm OX}(r)$ is shown in figure 10 and was obtained by adopting the same procedure that was used to find e.g. $\Delta G_{\rm D}(r)$ from $\Delta F_{\rm D}(Q)$. The first peak at 0.987(5) Å is attributed to intra-molecular O-X correlations, where X represents a weighted average of H and D, and gives a coordination number $\bar{n}_{\rm OX} = 2.0(1)$. The second peak at 1.83(2) Å arises from inter-molecular O-X correlations.

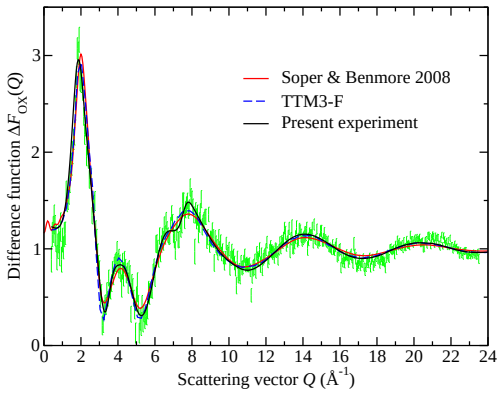

Figure 9. The second difference function $\Delta F_{\rm OX}(Q)$ as obtained from the present experiment (points with vertical (green) error bars), from the EPSR models of Soper and Benmore for heavy and light water [54] (solid light (red) curve), and from the path integral molecular dynamics simulations for heavy and light water using the TTM3-F model (broken dark (blue) curve). The solid dark (black) curve gives the Fourier back transform of the $\Delta G_{\rm OX}(r)$ function shown by the solid dark (black) curve in figure 10 where the unphysical oscillations at r values smaller than the distance of closest approach between the centres of two atoms are set to the calculated limit for $\Delta G_{\rm OX}(r = 0)$.

5.3. Weighted difference function $\Delta F_{\rm OO}(Q)$

The weighted difference function $\Delta F_{\rm OO}(Q)$ illustrated in figure 11 was constructed from the $\Delta F_{\rm D}(Q)$ and $\Delta F_{\rm H}(Q)$ functions shown in figures 4 and 5 by using equation (14). The same $\Delta F_{\rm OO}(Q)$ function was obtained, within the statistical errors, by fitting the difference $\{\Delta F'_{\rm D}(Q) - [b_{\rm D}\Delta F'_{\rm H}(Q)/b_{\rm H}]\}$ to the expression $\Delta P_{\rm OO}(Q) = a + bQ^2 + cQ^4$ and by combining the results according to equation (13). Provided that $S_{\rm OH}(Q)$ and $S_{\rm OD}(Q)$ largely cancel in the regions of interest, $\Delta F_{\rm OO}(Q) \simeq S_{\rm OO}(Q)$ such that $\Delta G_{\rm OO}(r) \simeq g_{\rm OO}(r)$. The $\Delta G_{\rm OO}(r)$ function is shown in figure 12. Integration of the first peak at 2.81(1) Å to a cutoff value of 3.25 Å gives a coordination number $\bar{n}_{\rm OO} = 4.1(1)$.

The results for $\Delta F_{\rm OO}(Q)$ are compared, in figure 11, with the partial structure factor $S_{\rm OO}(Q)$ as measured by using the method of neutron diffraction with H/D isotope substitution when employing the same diffractometer in the same setting as the present work [55]. The first peak in the corresponding partial pair distribution

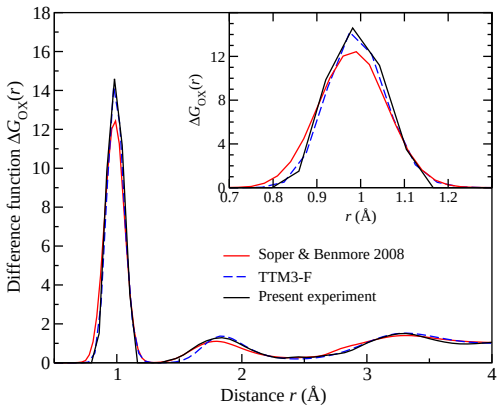

Figure 10. The second difference function $\Delta G_{\mathrm{OX}}(r)$ as obtained from the present experiment (solid dark (black) curve), from the EPSR models of Soper and Benmore for heavy and light water [54] (solid light (red) curve), and from the path integral molecular dynamics simulations for heavy and light water using the TTM3-F model (broken dark (blue) curve). The inset shows the region of the first peak in more detail.

function $g_{\mathrm{OO}}(r)$ (see figure 12) is at 2.82(1) Å and its integration to a cutoff value of 3.25 Å gives $\bar{n}_{\mathrm{OO}} = 4.2(1)$. The inset in figure 12 shows the x-ray total pair distribution function $G_{\mathrm{X}}(r)$ as measured for water at 299 K [5] and as obtained by Fourier transforming the x-ray total structure factor reconstructed from the full set of partial structure factors measured by using the method of H/D isotope substitution in neutron diffraction [55]. Since the atomic number for oxygen is larger than for hydrogen, $G_{\mathrm{X}}(r)$ will have a large contribution from O-O correlations. The nearest-neighbour peaks in the measured and reconstructed $G_{\mathrm{X}}(r)$ functions both occur at 2.81(1) Å and have comparable heights. The nature of the nearest-neighbour O-O correlations will be discussed in more detail in sections 7.1 and 7.3.

6. Path integral molecular dynamics results

The introduction of quantum (qm) effects to rigid or flexible harmonic classical (cl) models leads, in general, to a large de-structuring of the hydrogen bonded network as shown by (i) a decrease in height of the first peak in the O-O pair distribution function $\Delta h_{\mathrm{OO}}^{\mathrm{cl-qm}} = g_{\mathrm{OO}}(r)|_{\mathrm{max}}^{\mathrm{cl}} - g_{\mathrm{OO}}(r)|_{\mathrm{max}}^{\mathrm{qm}}$, which is an indicator of inter-molecular ordering, and (ii) an increase in number of hydrogen bonds broken, $\Delta \bar{n}_{\mathrm{OH}}^{\mathrm{cl-qm}} = \left(\bar{n}_{\mathrm{OH}}^{\mathrm{cl}} - \bar{n}_{\mathrm{OH}}^{\mathrm{qm}}\right)/\bar{n}_{\mathrm{OH}}^{\mathrm{cl}}$ (see table 1) [39, 56, 57, 58]. $\bar{n}_{\mathrm{OH}}$ is the first inter-molecular O-H coordination number such that $\Delta \bar{n}_{\mathrm{OH}}^{\mathrm{cl-qm}} > 0$ implies a breaking of bonds on including quantum effects. The replication of the peak height reduction $\Delta h_{\mathrm{OO}}^{\mathrm{cl-qm}}$ by using classical models requires an increase of the liquid temperature by $\Delta T \simeq$ 35–40 K. The de-structuring can have dramatic implications for the dynamics with the diffusion coefficient changing by as much as 50% [22, 39, 59]. By contrast, flexible anharmonic models and a recent first principles molecular dynamics study

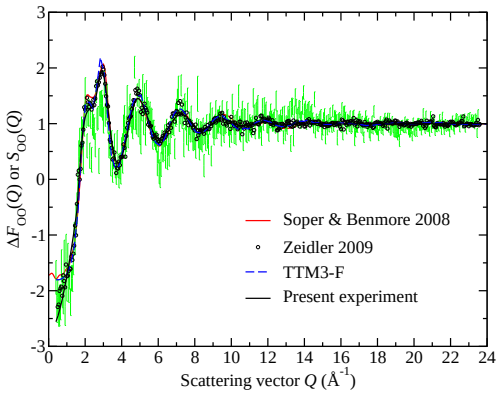

Figure 11. The weighted difference function $\Delta F_{\mathrm{OO}}(Q)$ as obtained from the method of neutron diffraction with oxygen isotope substitution (points with vertical (green) error bars), from the EPSR models of Soper and Benmore [54] for heavy and light water (solid light (red) curve), and from the path integral molecular dynamics simulations for heavy and light water using the TTM3-F model (broken dark (blue) curve). The solid dark (black) curve gives the Fourier back transform of the $\Delta G_{\mathrm{OO}}(r)$ function shown by the solid dark (black) curve in figure 12 where the unphysical oscillations at r values smaller than the distance of closest approach between the centres of two atoms are set to the calculated limit for $\Delta G_{\mathrm{OO}}(r = 0)$. A comparison is also made with the $S_{\mathrm{OO}}(Q)$ function as measured for water at 298(2) K by using the method of neutron diffraction with H/D isotope substitution (open circles) [55].

predict much smaller changes in the structure of water [4, 22], corresponding to $\Delta T \simeq$ 5–18 K.

As shown in table 1, the difference between the intra-molecular O-H and O-D bond lengths of 0.0054 Å or ≃0.5% found for the TTM3-F model is significantly larger than found for most empirical models, but is in excellent agreement with our diffraction data. For comparison, the model gives for the vapour phase of water in its ground vibrational state a difference between the O-H and O-D bond lengths of 0.0042 Å as compared to a measured value of 0.0037 Å [52]. It is worthwhile noting that the TTM3-F model was originally parameterized using *ab initio* calculations of gas phase clusters as opposed to experimental results and is therefore largely unbiased in its prediction of the liquid structure. The model also incorporates a great deal of flexibility into the form of the potential by the inclusion of anharmonic monomer flexibility as well as geometry dependent charges and polarisibility. The TTM3-F model reproduces accurately the O-H stretching region of the infra-red absorption spectrum of liquid water [40] and, when quantum effects are included, the diffusion coefficient $D_{\mathrm{qm}} = 0.95{\times}0.237 = 0.225$ Å^2 ps^{-1} is in excellent accord with the measured value of 0.229 Å^2 ps^{-1} [22, 40]. It has also recently been shown to give a good account of the two-dimensional and pump-probe infra-red spectra measured for dilute solutions of HOD in H_2O [53].

The results obtained from the path integral molecular dynamics simulations for the TTM3-F model are compared with the measured data sets in figures 4–6 and

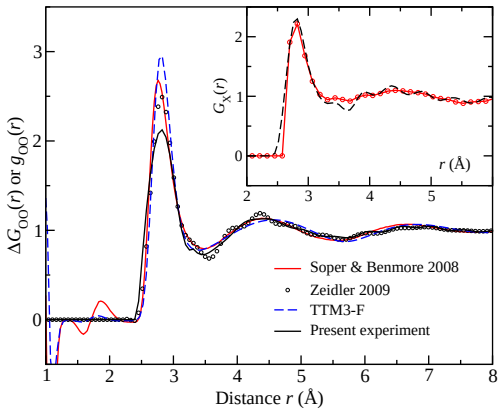

Figure 12. The weighted difference function $\Delta G_{\mathrm{OO}}(r)$ as obtained from the method of neutron diffraction with oxygen isotope substitution (solid dark (black) curve), from the EPSR models of Soper and Benmore [54] for heavy and light water (solid light (red) curve), and from the path integral molecular dynamics simulations for heavy and light water using the TTM3-F model (broken dark (blue) curve). A comparison is also made with the $g_{\mathrm{OO}}(r)$ function as measured at 298(2) K by using the method of neutron diffraction with H/D isotope substitution (open circles) [55]. The features at small r in the path integral molecular dynamics and EPSR results arise from a non-cancellation of the intra-molecular O-D and O-H partial pair distribution functions. The inset shows the x-ray total pair distribution function $G_X(r)$ as measured for water at 299 K (broken dark (black) curve) [5] and as obtained by Fourier transforming the x-ray total structure factor reconstructed from the full set of partial structure factors measured by using the method of neutron diffraction with H/D isotope substitution (solid light (red) curve with circles) [55].

9–12. In this comparison the path integral molecular dynamics results were treated in the same manner as the experimental data i.e. $\Delta F_{\mathrm{H}}(Q)$, $\Delta F_{\mathrm{D}}(Q)$, $\Delta F_{\mathrm{OX}}(Q)$ and $\Delta F_{\mathrm{OO}}(Q)$ were obtained from the simulated partial structure factors for light and heavy water by using equations (6), (10), (12) and (14), respectively. As shown in figure 6, there is good overall agreement between the measured and simulated intra-molecular peak positions and profiles for both $\Delta G_{\mathrm{D}}(r)$ and $\Delta G_{\mathrm{H}}(r)$. In the case of $\Delta G_{\mathrm{D}}(r)$, for which the measured first inter-molecular O-D peak is established as a robust feature (see figure 8), the experimental peak position is at 1.83(2) Å, the weighted peak position $\langle r_{\mathrm{OD}} \rangle = \int \mathrm{d}r\, r g_{\mathrm{OD}}(r) / \int \mathrm{d}r\, g_{\mathrm{OD}}(r)$ is at 1.93(2) Å, and the corresponding coordination number $\bar{n}_{\mathrm{OD}} = 2.2(2)$. By comparison, the simulation results for the first inter-molecular O-D peak and weighted peak positions are 1.84 and 1.91 Å, respectively. The simulated first inter-molecular O-H peak is at 1.84 Å with a weighted peak position of 1.91 Å i.e. the average length of a hydrogen bond barely changes between light and heavy water.

In table 2, the change predicted by path integral molecular dynamics simulations in the first inter-molecular coordination number $\Delta \bar{n}_{\mathrm{OX}}^{\mathrm{D-H}} = (\bar{n}_{\mathrm{OD}} - \bar{n}_{\mathrm{OH}}) / \bar{n}_{\mathrm{OD}}$ when H is substituted by D is compared for some common models of water. In this expression, $\bar{n}_{\mathrm{OH}}$ and $\bar{n}_{\mathrm{OD}}$ are the first inter-molecular O-H and O-D coordination numbers in H_2O and D_2O, respectively, such that $\Delta \bar{n}_{\mathrm{OX}}^{\mathrm{D-H}} > 0$ implies a breakage of

Table 1. The change in structure predicted for some common models of water when quantum mechanical effects are included by using path integral molecular dynamics [21]. The models are either rigid (R), flexible harmonic (FH) or flexible anharmonic (FA). The difference between the intra-molecular bond length on substituting H for D, $\Delta r = r_{\rm OH} - r_{\rm OD}$, is compared to (i) the difference in height of the first peak in the O-O partial pair distribution function, $\Delta h_{\rm OO}^{\rm cl-qm}$, and (ii) the fractional change in the number of hydrogen bonds, $\Delta \bar{n}_{\rm OH}^{\rm cl-qm}$, as calculated from classical (cl) versus quantum (qm) simulations for H_2O. $\Delta \bar{n}_{\rm OH}^{\rm cl-qm} > 0$ implies a breakage of bonds on including quantum effects. The inter-molecular O-H coordination numbers used to calculate $\Delta \bar{n}_{\rm OH}^{\rm cl-qm}$ were obtained by using equation (8) with an integration range defined by the minima on either side of the first inter-molecular O-H peak in $g_{\rm OH}^{\rm cl}(r)$. Also listed are ΔT (see the text) and the ratio of the quantum to classical diffusion coefficients $D_{\rm qm}/D_{\rm cl}$ for a given model of H_2O [22].

Model	Type	Ref.	Δr (Å)	$\Delta h_{\rm OO}^{\rm cl-qm}$	$\Delta \bar{n}_{\rm OH}^{\rm cl-qm}$ (%)	ΔT (K)	$D_{\rm qm}/D_{\rm cl}$
TIP4P	R	[36]	0	0.30	1.97	35	1.53
SPC/E	R	[37]	0	0.31	1.46	35	1.42
SPC/F	FH	[38]	0.0011	0.35	1.85	40	1.43
q-TIP4P/F	FA	[22]	0.0038	0.20	0.53	18	1.15
TTM3-F	FA	[40]	0.0054	0.03	-1.21	5	0.95

Table 2. The change in structure predicted by path integral molecular dynamics simulations for some common models of water when H is substituted by D. The models are either rigid (R), flexible harmonic (FH) or flexible anharmonic (FA). The difference between the intra-molecular bond length, $\Delta r = r_{\rm OH} - r_{\rm OD}$, is compared to (i) the difference in height of the first peak in the O-O partial pair distribution function, $\Delta h_{\rm OO}^{\rm D-H}$, and (ii) the fractional change in the number of hydrogen bonds, $\Delta \bar{n}_{\rm OX}^{\rm D-H}$, where $\Delta \bar{n}_{\rm OX}^{\rm D-H} > 0$ implies a breakage of bonds on changing from heavy to light water. The inter-molecular O-D and O-H coordination numbers used to calculate $\Delta \bar{n}_{\rm OX}^{\rm D-H}$ were obtained by using equation (8) with an integration range defined by the minima on either side of the first inter-molecular O-D peak in $g_{\rm OD}(r)$.

Model	Type	Ref.	Δr (Å)	$\Delta h_{\rm OO}^{\rm D-H}$	$\Delta \bar{n}_{\rm OX}^{\rm D-H}$ (%)
TIP4P	R	[36]	0	0.072	0.83
SPC/E	R	[37]	0	0.091	0.57
qSPC/Fw	FH	[39]	-0.0006	0.100	0.82
SPC/F	FH	[38]	0.0011	0.075	0.73
q-TIP4P/F	FA	[22]	0.0038	0.056	0.56
TTM3-F	FA	[40]	0.0054	0.003	-0.19

bonds on changing from heavy to light water. Table 2 also shows the corresponding change in height of the first peak in the O-O partial pair distribution function $\Delta h_{\rm OO}^{\rm D-H} = g_{\rm OO}(r)|_{\rm max}^{\rm D_2O} - g_{\rm OO}(r)|_{\rm max}^{\rm H_2O}$. The differences $\Delta \bar{n}_{\rm OX}^{\rm D-H}$ and $\Delta h_{\rm OO}^{\rm D-H}$ are smaller for TTM3-F by comparison with the other models.

7. Discussion

7.1. Comparison with Empirical Potential Structure Refinement (EPSR) results

It is worthwhile comparing the experimental results for water obtained in the present work with those obtained by Soper and Benmore [54] using the method of Empirical Potential Structure Refinement (EPSR). In this work the measured total neutron and x-ray structure factors for either light or heavy water at a temperature of 296–298 K were considered and atomistic configurations were initially generated by using the fixed charge rigid SPC/E model for water. The parameters describing the potential energy model were then changed in order to generate revised atomistic configurations for which the calculated structure factors are in agreement with the measured functions. Different starting models and the same measured data sets often lead to different conclusions with regards to the partial pair correlation functions [9]. Additionally, use is made of an arbitrarily chosen feedback (or "confidence") factor that weights the results either towards those obtained from the starting potential model, such that the extracted pair correlation functions are essentially those of the starting model, or towards the experimental data, such that the extracted pair correlation functions contain more information on the experimental results [62, 63]. In consequence, the extracted $S_{\alpha\beta}(Q)$ and $g_{\alpha\beta}(r)$ functions for a given set of data depend on the choice of confidence factor in addition to the starting model used for the refinement. Thus, in comparison with the present experimental work, the results of Soper and Benmore [54] were derived from an independent set of experimental measurements by using a rather different data analysis and interpretation procedure.

The EPSR generated first difference functions $\Delta F_{\rm D}(Q)$ and $\Delta F_{\rm H}(Q)$ are compared to the present experimental results in figures 4 and 5, respectively. The data sets are in agreement within the experimental error at most Q values. The EPSR results do, however, yield subtly different real space functions (figure 6) with a first peak in $\Delta G_{\rm D}(r)$ or a first trough in $\Delta G_{\rm H}(r)$ that is lower and wider than found in the present experimental work or in our path integral molecular dynamics simulations using the TTM3-F water model (this observation also holds for the first peak in $\Delta G_{\rm OX}(r)$ - see figure 10). The intra-molecular O-D and O-H bond distances deduced from the positions of these features are 0.97 and 1.01 Å, distances that increase to the values of 0.98 and 1.01 Å quoted in Ref. [54] if the first peak and trough positions are instead obtained from $r\Delta G_{\rm D}(r)$ and $r\Delta G_{\rm H}(r)$, respectively. This difference in the intra-molecular bond lengths of $\simeq$3% compares to a difference of $\simeq$0.4–0.5% found in the present experimental work for liquid water, for ice-Ih [50] or for the vapour phase [52]. It is also much larger than found in any theoretical prediction. For example, of the water models considered in the present paper, the TTM3-F model shows the greatest bond length change on going from H_2O to D_2O (tables 1 and 2). Since the mean square displacement of a quantum harmonic oscillator scales as $1/\sqrt{m}$, where m is the particle mass, an even larger bond length change is expected in going to the classical limit as $m \to \infty$ [64]. In this limit, the TTM3-F model shows an increase in bond length of 1.9% which is still smaller than seen in the EPSR modelled data.

The EPSR generated first inter-molecular O-D and O-H bond distances are $\sim$1.81 and $\sim$1.74 Å, respectively [54]. This O-D inter-molecular bond distance compares to a value of 1.83(2) Å obtained from the present experimental results for $\Delta G_{\rm D}(r)$ and with a value of 1.84 Å obtained from the path integral molecular dynamics results for the TTM3-F model. The latter do not, however, support the large difference in the

first inter-molecular O-D and O-H bond distances of ∼0.07 Å reported by Soper and Benmore [54] (see section 6). The EPSR results give first inter-molecular coordination numbers of $\bar{n}_{\rm OD} = 1.88(5)$ in D_2O and $\bar{n}_{\rm OH} = 1.81(5)$ in H_2O such that $\Delta\bar{n}_{\rm OX}^{\rm D-H} \simeq 0.04$. The corresponding values for several commonly used water models are listed in table 2.

The EPSR results were also used to reconstruct the second difference function $\Delta F_{\rm OX}(Q)$ by using equation (12) and a comparison with the present experimental results is made in figure 9. The data sets are found to be in agreement within the experimental error at most Q values. In real space, the first peak in $\Delta G_{\rm OX}(r)$ (figure 10) arises from a weighted average of the intra-molecular O-D and O-H correlations and its position is 0.987(5) Å (present experiment) or 0.98 Å (EPSR). The corresponding first peak positions in $r\Delta G_{\rm OX}(r)$ are 0.992(5) and 0.99 Å, respectively. Thus, although there is a difference between the individual intra-molecular O-D and O-H bond distances deduced from the present experiment and from EPSR, the weighted average intra-molecular O-X distances are the same within the experimental error. By comparison, the inter-molecular bond distance deduced from $\Delta G_{\rm OX}(r)$ is 1.83(2) Å (present experiment) or 1.80 Å (EPSR) while the corresponding values deduced from $r\Delta G_{\rm OX}(r)$ are 1.85(2) and 1.82 Å, respectively. There is therefore a small discrepancy between the weighted average inter-molecular O-X bond distances obtained from the present experiment and from EPSR.

The EPSR weighted difference function $\Delta F_{\rm OO}(Q)$, formed by using equation (14), is shown in figure 11 and the corresponding real space function $\Delta G_{\rm OO}(r)$ is shown in figure 12. The first peak positions in $\Delta G_{\rm OO}(r)$ and $r\Delta G_{\rm OO}(r)$ from EPSR are 2.76 and 2.77 Å, respectively. These distances are smaller than the values of 2.81(1) and 2.82(1) Å obtained from the $\Delta G_{\rm OO}(r)$ and $r\Delta G_{\rm OO}(r)$ functions measured in the present work, respectively, where the latter are found to be in agreement, within the experimental error, with the distances found from the other neutron and x-ray diffraction results described in section 5.3. The EPSR results give first O-O peak heights in $g_{\rm OO}(r)$ of 2.86 for D_2O and 2.59 for H_2O such that $\Delta h_{\rm OO}^{\rm D-H} \simeq 0.27$ which compares to 0.003 for the TTM3-F model (table 2).

7.2. Competing quantum effects in water

The quantitative agreement found between the present experimental results and the path integral molecular dynamics results for the TTM3-F model supports the proposal of "competing quantum effects" in liquid water [4, 22]. In this hypothesis inter-molecular zero point energy and tunnelling weaken the hydrogen bond network, as previously predicted [39, 56, 57, 58], but quantum fluctuations in the anharmonic intra-molecular O-H bond increase its length and hence the dipole moment of each water molecule. This higher dipole acts, in turn, to increase the binding between molecules and hence the net effect of quantum fluctuations is smaller than originally suggested from rigid water simulations. As shown in table 1 for a selection of water models, the extent of cancellation is strongly related to $\Delta r = r_{\rm OH} - r_{\rm OD}$, the change observed in the intra-molecular bond length on substituting H for D in the path integral simulations. The largest values of Δr correspond to flexible anharmonic models which show a much smaller change upon including quantum effects in (i) the O-O peak height, (ii) the number of hydrogen bonds broken, and (iii) the diffusion coefficient. In the case of the TTM3-F model, the cancellation between opposing quantum effects is large, leading to a fall in the O-O peak height of only 0.03 and a ratio of quantum to classical

diffusion coefficients of 0.95. These changes are much smaller than for rigid models which cannot exhibit any competition between intra-molecular and inter-molecular quantum effects. A large cancellation of competing quantum effects is fortuitous for experimental methods that exploit H/D isotope substitution such as the method of neutron diffraction with H/D isotope substitution [9, 10, 11, 12], two-dimensional infra-red spectroscopy [7, 8] and nuclear magnetic resonance (NMR) spectroscopy [60]. This is because when these methods are used to study systems involving either light or heavy water at 300 K the structural environments probed, as well as the quantum contribution to the dynamics, are likely to be similar.

7.3. The oxygen-oxygen correlations

As shown in figures 4 and 5 there are discrepancies between the experimental and path integral molecular dynamics results for the $\Delta F_{\rm D}(Q)$ and $\Delta F_{\rm H}(Q)$ functions in the region $\sim$1.5$-$3.5 Å^{-1} where these functions contain information on both the O-O and either the O-D or O-H correlations. In real space, the large r features in $\Delta G_{\rm D}(r)$ are established as robust (figure 8) and there are also discrepancies between the experimental and simulation results around the position of the first O-O peak at $\simeq$ 2.82 Å where the height of the experimental feature is smaller than for the simulation results obtained by using the TTM3-F model (figure 6). Any discrepancy at $\simeq$ 2.82 Å between experiment and simulation is smaller in the case of $\Delta G_{\rm OX}(r)$ (figure 10) which points to a first O-O peak height that is too large for the TTM3-F potential model. This observation is supported by the comparison made in figure 12 where the first O-O peak is also too high in the simulation as compared to experiment. All of this directs a way forward for improving models of water. For example, recent first-principles molecular dynamics simulations with van der Waals corrections predict peak heights in good agreement with those observed here [61].

We note that the intra-molecular O-D and O-X distances obtained from the present experimental work are 0.985(5) and 0.987(2) Å, respectively, while the first inter-molecular O-D and O-X distances are both 1.83(2) Å such that a linear O-D$\cdots$O or O-X$\cdots$O bond will take a value of 2.82(2) Å. The first peak in $\Delta G_{\rm OO}(r)$ occurs at 2.81(1) Å i.e. the average hydrogen bond is close to linear. By comparison, in ice-Ih crystallographic studies point to a linear hydrogen bond in both D_2O and H_2O [50], consistent with deuteron nuclear magnetic resonance spin alignment experiments which indicate a small bending of the hydrogen bond of about 3°, corresponding to an O-D$\cdots$O angle of $\simeq$177° [65]. The intra-molecular O-D and O-H distances deduced from a combination of crystallographic, nuclear magnetic resonance and spectroscopic results are 0.983(5) and 0.987(5) Å [50], respectively, which are in agreement with the distances that we obtain for water. Neutron and x-ray diffraction experiments give a hydrogen bonded O$\cdots$O distance of 2.75–2.76 Å [50, 51] which is shorter than in water, indicating larger cooperative effects [66]. The first inter-molecular O-D or O-H distance estimated from nuclear quadrupole resonance experiments on ice-Ih is 1.80(1) Å [50] yet, based on the O$\cdots$O and intra-molecular O-D or O-H distances in ice-Ih, a value closer to 1.77(1) Å is expected for a linear hydrogen bond.

8. Conclusions

The method of neutron diffraction with oxygen isotope substitution was successfully used to measure differences between the structures of light and heavy water that arise

from nuclear quantum mechanical effects. In particular, a difference of $\simeq 0.5\%$ was found between the intra-molecular O-D and O-H bond distances. The measured data sets are most consistent with the flexible anharmonic TTM3-F model for water which predicts an offset between intra-molecular and inter-molecular quantum contributions, thus supporting a competing quantum effects hypothesis for water under ambient conditions. The results indicate that the nearest-neighbour O-O peak height given by the TTM3-F model is too large, thus suggesting a way forward for its improvement.

Acknowledgments

We thank Hartmut Lemmel and Helmut Rauch (Vienna and Grenoble) for their input into the oxygen isotope scattering length measurements, Alain Bertoni (Grenoble) for helping with the diffraction experiments, David Manolopoulos (Oxford) for providing computer time for the simulations, and Alan Soper (ISIS) for providing the EPSR results. We also thank Werner Kuhs (Göttingen) for bringing his review on ice-Ih to our attention and for helpful discussions.

References

[1] Franks F 2000 *Water: A Matrix of Life* 2nd edn (Cambridge: Royal Society of Chemistry)
[2] Paesani F and Voth G A 2009 *J. Phys. Chem. B* **113** 5702
[3] Tomberli B, Benmore C J, Egelstaff P A, Neuefeind J and Honkimäki V 2000 *J. Phys.: Condens. Matter* **12** 2597
[4] Chen B, Ivanov I, Klein M L and Parrinello M 2003 *Phys. Rev. Lett.* **91** 215503
[5] Hart R T, Benmore C J, Neuefeind J, Kohara S, Tomberli B and Egelstaff P A 2005 *Phys. Rev. Lett.* **94** 047801
[6] Morrone J A and Car R 2008 *Phys. Rev. Lett.* **101** 017801
[7] Eaves J D, Loparo J J, Fecko C J, Roberts S T, Tokmakoff A and Geissler P L 2005 *Proc. Natl. Acad. Sci.* **102** 13019
[8] Loparo J J, Roberts S T and Tokmakoff A 2006 *J. Chem. Phys.* **125** 194522
[9] Soper A K 2000 *Chem. Phys.* **258** 121
[10] Soper A K and Ricci M A 2000 *Phys. Rev. Lett.* **84** 2881
[11] Dore J C, Garawi M and Bellissent-Funel M-C 2004 *Mol. Phys.* **102** 2015
[12] Soper A K 2007 *J. Phys.: Condens. Matter* **19** 335206
[13] Root J H, Egelstaff P A and Hime A 1986 *Chem. Phys.* **109** 437
[14] Neuefeind J and Benmore C 2009 *Nucl. Instrum. Methods Phys. Res. A* **600** 257
[15] Rauch H and Werner S A 2000 *Neutron Interferometry: Lessons in Experimental Quantum Mechanics* (Oxford: Clarendon)
[16] Zeidler A, Salmon P S, Fischer H E, Neuefeind J C, Simonson J M, Lemmel H, Rauch H and Markland T E 2011 *Phys. Rev. Lett.* **107** 145501
[17] Fischer H E, Simonson J M, Neuefeind J, Lemmel H, Rauch H, Zeidler A and Salmon P S (in preparation)
[18] Koester L, Rauch H and Seymann E 1991 *At. Data Nucl. Data Tables* **49** 65
[19] Sears V F 1992 *Neutron News* **3**(3) 26
[20] Rauch H and Waschkowski W 2002 *Neutron Data Booklet* ed A J Dianoux and G Lander (Grenoble: Institut Laue-Langevin) chapter 1.1.
[21] Parrinello M and Rahman A 1984 *J. Chem. Phys.* **80** 860
[22] Habershon S, Markland T E and Manolopoulos D E 2009 *J. Chem. Phys.* **131** 024501
[23] Li X-Z, Walker B and Michaelides A 2011 *Proc. Natl. Acad. Sci.* **108** 6369
[24] Fischer H E, Barnes A C and Salmon P S 2006 *Rep. Prog. Phys.* **69** 233
[25] Salmon P S, Xin S and Fischer H E 1998 *Phys. Rev. B* **58** 6115
[26] North D M, Enderby J E and Egelstaff P A 1968 *J. Phys. C.: Solid State Phys.* **1** 784
[27] Bertagnolli H, Chieux P and Zeidler M D 1976 *Mol. Phys.* **32** 759
[28] Paalman H H and Pings C J 1962 *J. Appl. Phys.* **33** 2635
[29] Soper A K and Egelstaff P A 1980 *Nucl. Instrum. Meth.* **178** 415
[30] Faber T E and Ziman J M 1965 *Phil. Mag.* **11** 153
[31] Powles J G 1981 *Mol. Phys.* **42** 757

[32] Soper A K 2009 *Mol. Phys.* **107** 1667
[33] Soper A K, Neilson G W, Enderby J E and Howe R A 1977 *J. Phys. C: Solid State Phys.* **10** 1793
[34] Enderby J E and Neilson G W 1981 *Rep. Prog. Phys.* **44** 593
[35] Enderby J E, Cummings S, Herdman G J, Neilson G W, Salmon P S and Skipper N 1987 *J. Phys. Chem.* **91** 5851
[36] Jorgensen W L, Chandrasekhar J, Madura J D, Impey R W and Klein M L 1983 *J. Phys. Chem.* **79** 926
[37] Berendsen H J C, Grigera J R and Straatsma T P 1987 *J. Phys. Chem.* **91** 6269
[38] Toukan K and Rahman A 1985 *Phys. Rev. B* **31** 2643
[39] Paesani F, Zhang W, Case D A, Cheatham III T E and Voth G A 2006 *J. Chem. Phys.* **125** 184507
[40] Fanourgakis G S and Xantheas S S 2008 *J. Chem. Phys.* **128** 074506
[41] Ceriotti M, Parrinello M, Markland T E and Manolopoulos D E 2010 *J. Chem. Phys.* **133** 124104
[42] Fanourgakis G S, Markland T E and Manolopoulos D E 2009 *J. Chem. Phys.* **131** 094102
[43] Fischer H E, Palleau P and Feltin D 2000 *Physica B* **276-278** 93
[44] Fischer H E, Cuello G J, Palleau P, Feltin D, Barnes A C, Badyal Y S and Simonson J M 2002 *Appl. Phys. A* **74** S160.
[45] Hughes D J and Harvey J A 1955 *Neutron Cross Sections* Report BNL 325 (Brookhaven: Brookhaven National Laboratory, USA)
[46] Yarnell J L, Katz M J, Wenzel R G and Koenig S H 1973 *Phys. Rev. A* **7** 2130
[47] Topping J 1972 *Errors of Observation and Their Treatment* (London: Chapman and Hall) p 91
[48] Lorch E 1969 *J. Phys. C: Solid State Phys.* **2** 229
[49] Salmon P S 2006 *J. Phys.: Condens. Matter* **18** 11443
[50] Kuhs W F and Lehmann M S 1986 *Water Science Reviews 2* ed F Franks (Cambridge: Cambridge University Press) p 1
[51] Floriano M A, Klug D D, Whalley E, Svensson E C, Sears V F and Hallman E D 1987 *Nature* **329** 821
[52] Cook R L, De Lucia F C and Helminger P 1974 *J. Mol. Spectrosc.* **53** 62
[53] Paesani F 2011 *J. Phys. Chem. A* **115** 6861
[54] Soper A K and Benmore C J 2008 *Phys. Rev. Lett.* **101** 065502
[55] Zeidler A 2009 *Ordering in Amorphous Binary Systems* PhD thesis (Bath: University of Bath, UK)
[56] Kuharski R A and Rossky P J 1985 *J. Chem. Phys.* **82** 5164
[57] Wallqvist A and Berne B J 1985 *Chem. Phys. Lett.* **117** 214
[58] Hernández de la Peña L and Kusalik P G 2004 *J. Chem. Phys.* **121** 5992
[59] Hernández de la Peña L and Kusalik P G 2006 *J. Chem. Phys.* **125** 054512
[60] Cui X, Mao S, Liu M, Yuan H and Du Y 2008 *Langmuir* **24** 10771
[61] Wang J, Román-Pérez G, Soler J M, Artacho E and Fernández-Serra M-V 2011 *J. Chem. Phys.* **134** 024516
[62] Soper A K 2004 *Pramana J. Phys.* **63** 41
[63] Soper A K 2005 *Phys. Rev B* **72** 104204
[64] Atkins P W 1998 *Physical Chemistry* 6th edn (Oxford: Oxford University Press)
[65] Fujara F, Wefing S and Kuhs W F 1988 *J. Chem. Phys.* **88** 6801
[66] Kuhs W F and Lehmann M S 1987 *J. Physique Colloque* **48** C1-3